Coronal Mass Ejections: Overview

H. S. Hudson
Space Sciences Laboratory, University of California, Berkeley, CA 94720 USA

J.-L. Bougeret
Observatore de Paris, Meudon

J. Burkepile
High Altitude Observatory, Boulder

1. Background information

A Coronal Mass Ejection (CME; see Figure 1) is "...an observable change in coronal structure that 1) occurs on a time scale of a few minutes and several hours and 2) involves the appearance and outward motion of a new, discrete, bright, white-light feature in the coronagraph field of view" (Hundhausen et al., 1984; Schwenn, 1996). With a kinetic energy that may exceed 10^{32} ergs, it is one of the most energetic forms of solar activity. We believe a CME at essence to be the eruption of a magnetically closed volume of the lower and middle corona.[1] The CMEs are interesting in their own right; they also have substantial effects on the Earth's environment. In this Chapter we give an overview of the CME phenomenon, touching on all of its manifestations – traceable now from the photosphere into the distant heliosphere as far as human exploration has extended. This Chapter summarizes the basic knowledge available prior to the Workshop. Figure 1 shows representative examples.

Originally termed "coronal transients", CMEs entered the modern era (but see Figure 1 for an historical observation) with the Skylab observations (Gosling et al., 1974; Munro et al., 1979). The detailed records provided by the P78-1 coronagraph (Howard et al., 1985) provided an early comprehensive view, including the discovery of the "halo CME" (Howard et al., 1982) now known to be mainly responsible for terrestrial effects.

The modern view of CMEs has broadened considerably as the result of observations made by instruments other than coronagraphs at visual wavelengths. The Chapman Conference of 1997 (Crooker et al., 1997)

---

[1] In our usage the lower and middle corona are below and above, respectively, the projected height of a typical coronagraphic occulting edge.
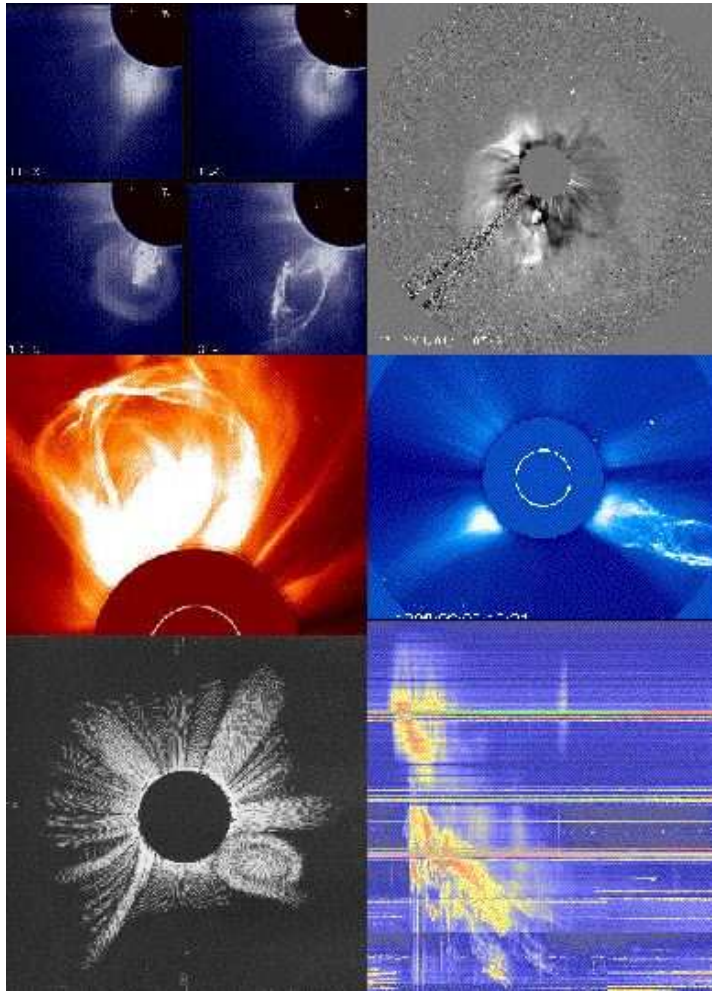
Figure 1. Six views of coronal mass ejections. Top: Prototypical "3-part CME" as observed by SMM; halo CME from LASCO. Middle: two views of flux-rope CMEs (LASCO). Bottom: Historical eclipse observation of possible CME; type II radio burst (Culgoora).

provides an excellent set of papers covering both the classical and the newer material available then.

The solar corona consists mainly of hot (10^6 K) and ionized plasma, bounded above by the solar wind and below by atmospheric layers at much lower temperatures. The magnetic field dictates the structure of the corona, according to its generally low plasma beta (the ratio of gas to magnetic pressure; see Figure 2). CME movies give the impression that a sector of the coronal field simply expands and opens out
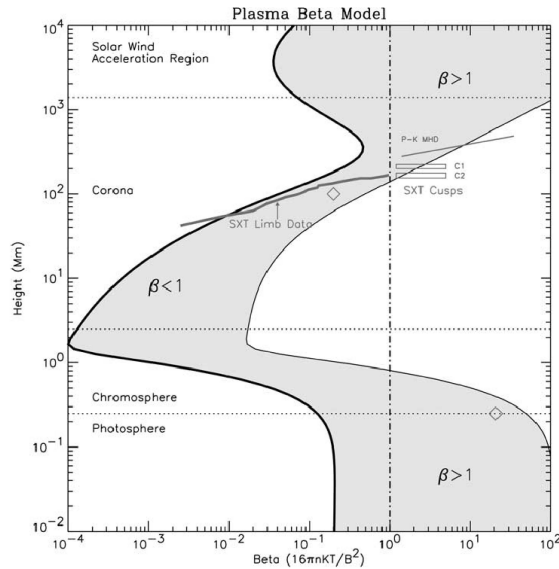
Figure 2. Survey of coronal plasma β, from Gary (2001), as a function of height above the photosphere. Note that this display ignores non-radial variation. A similar plot for Alfvén speed would show a radial decrease outward, followed by a rise to a local maximum in the upper corona, then a monotonic decline into the heliosphere.

into the solar wind. It thus (temporarily. at least) must increase the open-field fraction of the photospheric field. The corona (to 10 R$_\odot$) contains 10^{18-19} g according to the semi-empirical models of Withbroe (1988). The mass content above 3 R$_\odot$, representative of the domain of coronagraphic observations, would not amount to 10^{15} g in the angular domain of a large CME, so that (as the images show) most of the CME mass typically originates in or below the lower corona.

Figure 2 shows estimates of the distribution of β with height; generally above an active region we expect lower values because of the exponential density decrease (e.g., Gary, 2001). Our direct knowledge of the coronal magnetic field is extremely limited because of observational difficulties. As a result one must use representative ranges (as presented in Figure 2) or extrapolations from the photospheric Zeeman-splitting observations, usually based on the force-free condition $\nabla \times B = \alpha B$ (where α generally would be a function of position as determined by subphotospheric conditions). These extrapolations have systematic errors, the most obvious of which is that the photospheric observations refer to a layer that is not itself force-free.

In general the corona supports a system of currents, and so potential-field representations based upon data at the lower boundary cannot

exactly represent the geometry. The "potential field source surface" (PFSS) method ingeniously sidesteps this problem (Altschuler and Newkirk, 1969, Schatten et al., 1969), at least for the large-scale structure. In this approach one uses a potential representation from the photosphere out to an optimum spherical "source surface," almost universally now set at 2.5 R$_\odot$. A fictitious current system flows on this surface with such a distribution that the field external to it is strictly radial. Several groups pursue this practical approach, which (for example) appears to do a good job in defining coronal holes and open field for heliospheric applications (e.g., Wang et al., 1996). Unfortunately it cannot be used to represent magnetic energy storage within the coronal domain itself, so it is of little use in studying the details of flare or CME evolution.

The photospheric magnetic field does not reflect CME occurrence in any obvious way, although observations of subtle flare effects do exist, especially in limb observations where a small tilt in the field may affect the line-of-sight component (Cameron and Sammis, 1999). This absence of strong effects is consistent with the general idea of coronal energy storage and release to explain the transients, but this conclusion must be understood more quantitatively. It is also consistent with the important idea (Melrose, 1995) that the vertical currents responsible for coronal magnetic energy storage must have their origin deep in the convection zone, and not vary appreciably during the transient.

CMEs usually come from active regions in close association with major solar flares, but they also can come from filament channels in the quiet Sun. The three-part structure for the quiet-Sun events, often associated with filament eruptions from the polar crown, can be directly identified with the appearance of a streamer cavity seen on the limb in white light or soft X-rays. Quiet-Sun events correspond to weak flare-like effects seen in chromospheric observations (Harvey et al., 1986); such events often have slow, low-temperature soft X-ray emissions that do not produce recognizable GOES[2] signatures (e.g., Hudson et al., 1995).

2. Techniques of observation

CMEs are observed directly by white-light coronagraphs, mostly via photospheric light Thomson-scattered by coronal electrons. Eclipse images show coronal structure definitively well, and in spite of their infrequency have shown CMEs in rare historical cases (see Figure 1). Phenomena related to CMEs appear at virtually every observable wave-

---

[2] Geostationary Operational Environmental Satellite

length (the "non-coronagraphic" observations; see Hudson and Cliver, 2001) as well as in many interplanetary signatures (e.g., Gosling, 1991).

Optical/UV. Lyot's invention of the coronagraph permitted time-series observations of changes in coronal structure. A coronagraph is a special-purpose telescope that images only the corona, suppressing the bright photosphere by either internal or external occultation; stray-light levels can now be reduced to the order of 10^{-15} of disk brightness at an elongation of $18°$ (Buffington et al., 2003). The essential point of the visible-light observations is that they show the electron-scattered emission of the K-corona; the intensity thus determines the line-of-sight column density of the corona, which is optically thin outside prominences. The high temperature of the corona smears out the photospheric Fraunhofer line spectrum, but an emission-line component appears prominently at short wavelengths.

Radio. Within the vast spectral range of ground-based radio techniques (roughly 3×10^6 Hz to 10^{12} Hz) one finds a variety of emission mechanisms and observing techniques. The meter-decimeter wavelength ranges show us the corona mainly via coherent emission mechanisms; because these are bright at the plasma frequency one gets a rough measure of the density. At shorter wavelengths the optical depth decreases until at submillimeter wavelengths one sees right into the upper photosphere. Free-free emission can be detected either from over-dense coronal loops following flares, or the quiet lower solar atmosphere; gyrosynchrotron radiation comes from high-energy electrons. Below about 10 MHz radio receivers in space allow us to study solar-wind phenomena as far down as the local plasma frequency at one A.U., normally at $\sim 3 \times 10^4$ Hz.

EUV/X-ray. The EUV and X-ray wavelengths show us the K-corona directly in emission. The emissivity of the hot corona decreases rapidly at short wavelengths, but the extreme temperature dependence ($\propto \mathrm{e}^{-h\nu/kT}$ in the limit) results in very large image contrast for X-rays at $h\nu > kT$. Focusing optics (grazing incidence for soft X-rays to a few keV; normal incidence for narrow-band imaging longward of about 100Å) with good angular resolution led to many discoveries from the first systematic X-ray and EUV observations, those from *Skylab*, and then from *Yohkoh*: coronal holes, flares, CME-related ejecta and dimmings, and in general many counterparts of phenomena previously studied only at radio wavelengths. The normal-incidence TRACE observations have revolutionized our views of coronal dynamics, owing to their high resolution ($0.5''$ pixels; see Handy et al., 1999).

Interplanetary. The interplanetary data mostly consist of *in-situ* measurements of particles and fields, in which one characterizes the bulk parameters (speed, density, temperature) of the solar wind, plus

the distribution functions and abundances (ionization states, elements, isotopes) within the plasma. These include solar energetic particles resulting ultimately from flares and CMEs; the interplanetary shock waves have a close association with CMEs (Sheeley et al., 1985), and these shock waves cause SEP (Solar Energetic Particle) events (e.g., **?**, **?**). Most of the interplanetary observations are from near-Earth space, but *Helios*, *Ulysses*, and the Voyagers have now explored as far in as 0.3 R$_\odot$, out of the ecliptic plane, and out to the heliopause.

3. CMEs: coronagraphic observations

3.1. WHITE LIGHT

CMEs are unambigously identified in white light coronal observations as outward-moving density structures (Tousey, 1973; Gosling et al., 1974). The rate at which they occur correlates well with the solar activity cycle (Webb and Howard, 1994; St. Cyr et al., 2000); their appearance does not significantly differ between sunspot minimum and sunspot maximum. CMEs often appear as a "3-part" structure comprised of an outer bright *front*, and a darker underlying *cavity* within which is embedded a brighter *core* as shown in Figure 1. The front may contain swept-up as well as primary material (Hildner et al., 1975; Illing and Hundhausen, 1985). The cavity is a region of lower plasma density but probably higher magnetic field strength. The cores of CMEs can often be identified as prominence material on the basis of their visibility in chromospheric emission lines (Sheeley et al., 1975; Schmieder et al., 2002) and often appear to have helical structure.

In addition to the familiar 3-part CMEs, other types commonly occur – narrow CMEs and CMEs with clear flux-rope morphology, in particular (Howard et al., 1985). Halo CMEs (Figure 1) have special properties resulting from projection effects; see Burkepile et al. (2004).

Five different satellites or observatories have contributed substantial information about CME properties in a statistical sense: *Skylab*, Solwind, SMM, and SOHO from space, and the MK3 coronagraph at Mauna Loa Solar Observatory. These instruments have different properties (sampling, radius of occulting edge, epoch of observation) but a consistent picture generally prevails. We can distinguish the observational properties of CMEs into *morphological* (geometry, kinematics) and *physical* (mass, energy) categories. For reference we quote the average properties from the different sources in Table I; these are roughly consistent among the different data sets.

It is important to note that these are measurements of CME apparent properties as seen projected in two dimensions in an optically thin

Table I. CMEs: Average Properties

	MK3[a]	SMM[b]	Skylab[c]	Solwind[d]	LASCO[e]
Period of observation	1980-99	1980 1984-89	1973-1974	1979-1980 1984-85	1996- present
FOV (R$_\odot$)	1.15-2.24	1.8- 5	2-6	3-10	1.1-32
Angular Size (deg)	37	47	42	43	72
Speed (km/s)	390	349	470	460	424
Mass (g)		3.3×10^{15}	4.7×10^{15}	4.0×10^{15}	1.7×10^{15}
K. E. (ergs)		6.7×10^{30}	3.1×10^{30}	3.4×10^{30}	4.3×10^{30}
P. E. (ergs)		7.1×10^{30}	8.0×10^{30}		

[a] St. Cyr et al., 1999
[b] Hundhausen, 1993
[c] Gosling et al., 1976; Rust, 1979; Hundhausen, 1993
[d] Howard et al., 1985; Howard et al., 1986
[e] St. Cyr et al., 2000; Vourlidas et al., 2002

medium. This projection introduces systematic distortions in the appearance of the object and makes the determination of point properties more difficult and generally model-dependent. The distortions are small for structures close to the "plane of the sky" (i.e., the plane containing the solar limb) but can be severe elsewhere. Objects located away from the plane of the solar limb appear at higher apparent latitudes, have larger apparent widths and lower apparent heights than their true values (Hundhausen, 1993). In addition, the lower apparent heights lead to underestimates of CME speeds (Hundhausen et al., 1994). The underestimation of the height also impacts the brightness, and hence the mass estimate.

3.2. Morphological and kinematical properties

Position angles. The apparent latitude of a CME is typically determined from the position angle of its projected angular centroid (Howard et al., 1985). Hundhausen (1993) showed that this depends strongly upon the CME source location. They also found the distribution of apparent latitudes of CMEs to be unimodal and to center at the helio-magnetic equator. There is a systematic variation with the solar cycle. Around solar minimum the CMEs tend to occur at lower latitudes, and as the rise to maximum occurs, the apparent latitudes increase. The CME apparent latitudes are well correlated with the latitude distribution of the helmet streamers (Hundhausen, 1993), rather than with the "butterfly diagram" latitudes of active regions. The LASCO observa-
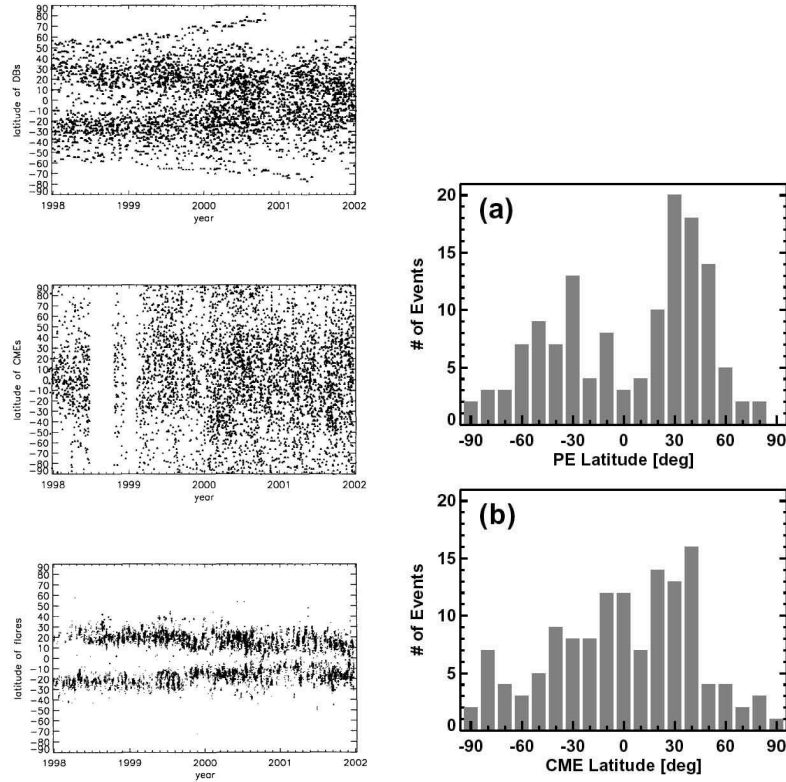
Figure 3. Left: Apparent latitudes (position angles) of CME occurrence, as observed by SOHO (center panel) compared with disappearing filaments (top) and flares (bottom) (from Pojoga and Huang, 2003). Right: Similar comparison between microwave-observed filament locations (top) and their corresponding CMEs (Gopalswamy et al., 2003). The statistical views show that CME origins in the low corona (flares or CME eruptions) have a bimodal distribution in latitude, whereas the CMEs have a unimodal distribution concentrated at the equator.

tions of the current cycle (St. Cyr et al., 2000) confirm this observation (Figure 3).

Angular sizes. The smallest average CME angular size in Table I is measured in the low coronal measurements from MK3 (St. Cyr et al., 1999). This suggests that some CMEs may expand in the early stages of their formation and propagation, particularly those events (the majority; see Subramanian and Dere, 2001) that originate in and near active regions (Dere et al., 1997). The higher average angular sizes determined from the outer coronal observations from LASCO (St. Cyr et al., 2000) probably results from projection since the LASCO coronagraphs are able to detect many disk-centered CMEs with large apparent widths.
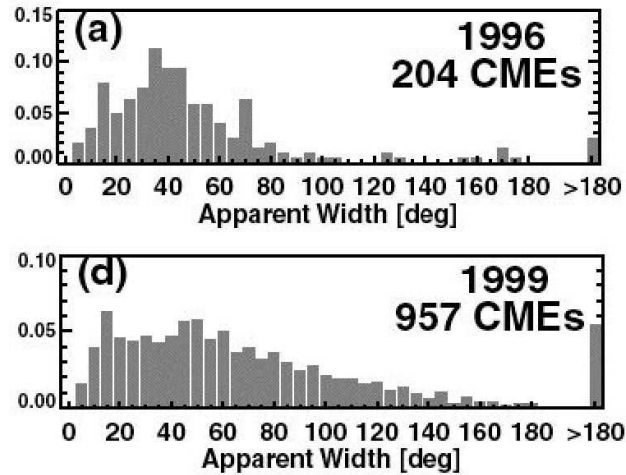
Figure 4. Angular sizes of CMEs vs. phase in the solar cycle, based upon LASCO observations (St. Cyr et al., 2000). The numbers of wider CMEs increases towards the solar maximum (Hundhausen, 1993).

Figure 4 compares CME apparent widths betwen states of low and high solar activity (St. Cyr et al., 2000). The data generally indicate a decrease in the percentage of wide CMEs during the descending or minimum phases of the solar cycle for each of the three datasets.

Speeds. The average CME speeds determined from the various datasets do not vary significantly (See Table I). This speed does however have a solar-cycle dependence, though not a simple one. Both SMM and Solwind report very low speeds for CMEs in 1984, during the declining phase of activity. However, the average SMM CME speeds are higher in 1985 and 1986, at solar minimum, due to the appearance of new active regions which are associated with a handful of high-speed CMEs. The lowest average LASCO CME speed occurs at solar minimum (1996) and gradually increases through 1998 with the appearance of a high-speed tail in the distribution which may be associated with the occurrence of new-cycle active regions. CMEs associated with active regions have higher average speeds than CMEs associated with eruptive prominences located away from active regions (Gosling et al., 1976).

Accelerations. MacQueen and Fisher (1983) found that CMEs associated with flares had more rapid accelerations. Sheeley et al. (1999), on this basis, argue for the existence of two types of CMEs: those associated with flares, which tend to appear at full speed and then decelerate, and the filament-eruption CMEs, which slowly accelerate (see Figure 5 for an example of the difference).
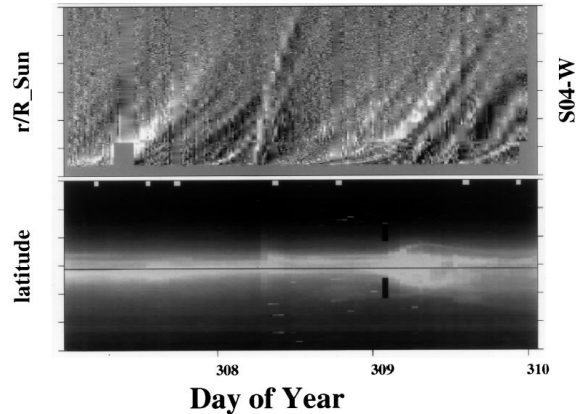
Figure 5. Illustration of the two types of CME suggested by Sheeley et al. (1999). The upper panel shows brightness distribution along a radial line (in this case 4° N of W, or a position angle of 274°). The decelerating event of Nov. 4, 1997, occurs early on Day 308 and was associated with an X2.1 flare at S14, W33. Many accelerating events can be seen as well.

3.3. Physical properties

Masses. The excess brightness of a given image relative to a pre-event image gives a "snapshot" estimate of CME mass via the plane-of-the-sky assumption. This represents a lower limit, and a snapshot also does not capture the continuing enhanced flow often seen long after the initial eruption. Standard assumptions are (1) that all of the CME material is located in the plane of the sky, and (2) that the corona is a completely ionized plasma consisting of 90% hydrogen and 10% helium by number (Vourlidas et al., 2000).

Energies. The kinetic and potential energies of a CME can be determined from the inferred masses and velocities, subject to the projection biases. The total mechanical energy of a major CME obtained in this manner is of order 10^{31-32} ergs, with the potential energy dominating for flux-rope CMEs (Vourlidas et al., 2000). The magnetic energy of a CME is the dominant factor; it is widely agreed that CMEs result from a conversion of magnetic energy into the other forms, but we have no direct observations and cannot confirm this. The energetics estimates of Vourlidas et al. (2000) suggest that the magnetic energy did in fact diminish as the kinetic and potential energies increased.

There are inherent inaccuracies in the estimates of CME energetics. CME masses are underestimated, due to the assumption that all of the material lies in the plane containing the solar limb. CME mass and speed underestimates become significant for CME components more

than ∼30 degrees from the plane of the solar limb (see Hundhausen 1993, Appendix A and Hundhausen et al. 1994).

Energy or mass distribution. Because the lack of direct estimates of the dominant component, the magnetic energy, it is doubtless premature to draw conclusions from the distribution of CME total energies, but the masses and kinetic energies are available. Vourlidas et al. (2002) suggest power-law distributions for the mass and kinetic energy, rather than an the exponential distribution of Jackson and Howard (1993). The inferred power laws are flatter than those observed for flares (e.g., Hudson, 1991).

3.4. UV and EUV Limb Spectroscopy

The UV and EUV spectrographic observations of CMEs provide diagnostic information but suffer from limited sensitivity. SOHO carries two UV spectrographs (UVCS for coronal observations, and SUMER for disk observations, but operated for most of the mission with its slit positioned above the limb in a coronagraphic mode).

Raymond et al., 2003 discuss three well-observed CMEs, each associated with an X-class flare near the limb The UVCS observing slit was positioned approximately tangent to the limb at a height of 1.64 $R_\odot$ above it, and with an observing cadence of 120 s for spectra of a variety of UV emission lines, including some with high formation temperatures (notably FeXVIII above 6×10^6 K). This high-temperature emission occurs in narrow structures the authors identify with the current sheets expected to form after the eruption (Ciaravella et al., 2002; Ko et al., 2003).

SUMER has provided observations that may be more directly related to flare energy release in large-scale reconnection. The original observation of downflows in soft X-rays by McKenzie and Hudson (1999) suggested reconnection outflow with a complex structure and clearly sub-Alfvénic velocities. SUMER observations have confirmed that the principal components of these downflows have low densities, being undetectable in any temperature regime (Innes et al., 2003).

4. CMEs: non-coronagraphic observations

Much of the interesting development of a CME takes place in the lower corona, below the coronagraph's occulting edge. Even if this edge could be placed exactly at the solar limb, a halo CME originating at disk center would be at a large radial distance from the Sun before any part of it became visible. Luckily there are many wavebands, ranging

from radio to X-ray, that in principle reveal the CME development from the photosphere outwards. One must be cautious interpreting these non-coronagraphic observations, because they show aspects of the CME disturbance that may not be directly identifiable with the mass distribution as seen in a coronagraph. Radio observations in particular normally show only non-thermal particles and thus give a picture of the overall structure that is biased towards those parts containing energetic particles, specifically electrons far out in the tail of the velocity distribution function. The "calibration" of these different kinds of observation presents problems to the extent that we may need to rely upon theory and modeling (or even cartoon descriptions) to link one feature with another observed by very different means (Hudson and Cliver, 2001).

4.1. X-ray and EUV imaging

We have now had more than a decade of systematic exploration of the solar corona via soft X-ray and EUV imaging from *Yohkoh*, SOHO, and TRACE. These new data have gone far beyond the pioneering observations from *Skylab*, especially in terms of sensitivity and of sampling. The essential contributions of these new observations lie in several domains: the *direct observation of ejecta* (Klimchuk et al., 1994; Nitta and Akiyama, 1999); the detailed observation of *coronal dimming* (Hudson and Webb, 1997); and the observation of *EIT waves* (Moses et al., 1997; Thompson et al., 1999). Such observations show that the coronal restructuring underlying the CME phenomenon in fact extends throughout the corona, consistent with the simple idea that the CME simply opens the coronal magnetic field into an enhanced solar-wind flow. Spectroscopic observations from SOHO (Harra and Sterling, 2001; Harrison et al., 2003) confirm that the X-ray dimmings do represent material depletions, rather than a temperature effect (Hudson et al., 1996).

The X-ray and EUV observations of eruptions should be considered in the context of the behavior of Hα filaments. Filaments give a different glimpse at coronal behavior during the CME process. The onset of filament activity, together with a gradual rising motion presumably related to streamer swelling, may precede the actual eruption by tens of minutes. In some cases the erupting filament continues into the outer corona, where it forms the dense core of a classical three-part CME structure; in other cases the filament appears to stop ("confined explosion" or failed eruption," see e.g. Moore et al., 2001; Ji et al., 2003), and in some CMEs there appears to be no filament involvement at all. The X-ray observations (Kano, 1994; Hanaoka et al., 1994) show that the filament matter may heat rapidly during the eruption, and the

EUV observations often show both cool and hot phases of the filament during its eruption.

The direct observations of CME counterparts in the low corona help greatly with understanding the time sequence of the eruption. The X-ray dimmings could be directly interpreted as a part of the coronal depletion required for a CME (Hudson et al., 1996; Sterling and Hudson, 1997; Hudson and Webb, 1997). The dimmings turned out to coincide with the flare brightening, suggesting that the flare energization and CME acceleration could be identified (Zarro et al., 1999). This close timing relationship has also been found with the LASCO C1 observations, which have the lowest occulting edge and hence the least timing ambiguity (Zhang et al., 2001).

Large-scale waves in the corona and heliosphere play a major role in any discussion of CMEs (Schwenn, 1986); indeed the CME disturbance itself is describable in terms of MHD waves (e.g., Chen et al., 2002). The type II bursts provided the first evidence for the passage of global waves through the corona and heliosphere, and the Moreton waves in the chromosphere (e.g., Athay and Moreton, 1961) were put into the same context by the Uchida (1968) theory of weak fast-mode MHD shock emission from solar flares. Interplanetary shocks and geomagnetic impulses (e.g. Chapman and Bartels, 1940) have on the other hand a natural interpretation in terms of bow shocks driven ahead of the CME ejecta.

4.2. Radio signatures

Radio-frequency observations provided some of the first clues large-scale restructuring of the solar corona during a CME. The metric wavelength band (30-300 MHz) led to the well-known event classification (the type I–V bursts; see Kundu, 1965). Space-borne receivers extended the observational domain down to ∼30 kHz, whereas at shorter wavelengths ground-based observations have become better and better. These bursts tell us about energetic electrons either trapped in large-scale coronal magnetic structures, or propagating through them on open field lines; in particular the type II bursts reveal MHD shock waves propagating away from coronal disturbances such as flares and CMEs. We also now have clear observations of the elements of the classical 3-part CME structure via gyrosynchrotron emission at decimetric wavelengths and via free-free emission at centimetric wavelengths (Bastian et al., 2001).

The radio observations provide key information about the connectivity of the coronal magnetic field. The type III bursts show that open (i.e., heliospheric) magnetic fields can originate in active regions as well

as in coronal holes; the exciter (an electron beam) can be traced over at least four decades in frequency or 8 decades of density.

4.3. *In-situ* MEASUREMENTS

Solar ejecta, including CMEs, often have observable consequences further out in the heliosphere. There is still no consensus regarding the mapping of features seen in (coronagraphic) CME observations with the interplanetary phenomena (Interplanetary CMEs, or ICMEs; see Schwenn, 1995), but there are many specific signatures (e.g., Gosling and Forsyth, 2001). These range from magnetic clouds (Burlaga et al., 1982), with a highly organized flux-rope magnetic pattern, to solar energetic particles (SEPs), whose acceleration is directly related to CME dynamics but which are observed on field lines not directly a part of the solar ejecta. The presence or absence of particular signatures varies from event to event, but counter-streaming electrons (i.e., suprathermal electrons with pitch-angle distributions aligned both parallel and antiparallel to the field) are commonly interpreted as indicating that the connectivity of the field is "closed" (here meaning tied to the Sun at both ends, hence the result of an ejection), even though the observations are carried out in the heliosphere (hence "open" from the solar-wind point of view).

The prevalence of flux-rope signatures in ICMEs, which are especially clear in the *Ulysses* high-latitude events (Gosling et al., 1995), strongly suggests several aspects of the solar imaging observations. It is now clear that the "disconnection" events long sought in coronagraphic signatures are rare, but the common occurrence of concave-up structures points instead to flux ropes formed in the corona. Such structures may be latent within streamers, or may be formed during the eruption according to the standard reconnection model – we do not yet know which – or possibly examples of both cases occur. Whereas we cannot detect the magnetism of streamers directly, coronal imaging is consistent with a structure consisting of elongated fields nearly parallel to the surface filling a cavity beneath overlying shorter closed field lines. This arcade-like field, the cavity, and the filament that may be suspended within the streamer strongly suggest the three-part structure of many CMEs.

The ICME magnetic properties can in principle be used to learn about the source regions of CMEs (Bothmer and Schwenn, 1994; Rust and Kumar, 1996; Cremades and Bothmer, 2004). Although we do not yet have a complete understanding of the mapping of ICME components to structures in the low corona, filament channels often play an important role. The prevalence of forward-reverse shock pairs in high-

latitude ICMEs, an indication of overexpansion (Gosling et al., 1994) is consistent with the non-radial expansion observed in the low corona by many techniques (e.g., Cremades and Bothmer, 2004). The particles observed within a CME can also be used as tracers of the magnetic connectivity (Kahler and Reames, 1991; Larson et al., 1997); the nearly relativistic particles at higher energies are especially interesting because of their short propagation times. The observations of impulsive particle events closely associated with flares (e.g., Kahler et al., 2001) confirms the knowledge from radio type III bursts that open (i.e., connected into the solar wind) field lines commonly occur in active regions near sunspots.

5. Overview of theory

The theory of coronal mass ejections involves a complicated system with large parameter ranges and an ill-understood coupling between large and small scales during the process of eruption. Accordingly the existing theories (e.g., Forbes, 2000) are more descriptive than predictive in nature (see Figure 6 for a cartoon representation given by Forbes, adding swept-up mass and a bow shock to the eruptive-flare cartoon of Hirayama (1974) and Anzer and Pneuman, 1982). Much of the theoretical work must be carried out in large-scale numerical simulations, and the scale of the problem unfortunately limits them to the (resistive) MHD approximation and to scales far larger than those thought necessary to capture the microscopic physics.

Most modern models invoke magnetic energy storage in the corona, which is released either by a dissipative process or by an ideal MHD loss of equilibrium in a low-β environment. Other models invoke direct driving by injection of twist from below the photosphere during the eruption; still others make use of gravitational energy stored in or above the erupting medium. In the dissipative models one describes the restructuring in terms of magnetic reconnection, either below the erupting structure ("tether cutting" or "emerging flux") or above it ("breakout"; Antiochos et al., 1999). These models would share the geometry of Figure 6 but would differ in the initiation mechanism. Many observational papers strive to identify these processes, but it would be fair to say that the current results are ambiguous. One grave problem with essentially all of the models is that they remain in the MHD framework and thus cannot deal self-consistently with energetic particles.

Finally, the fact of CME existence leads to several further interesting theoretical problems relating to their propagation into the heliosphere.
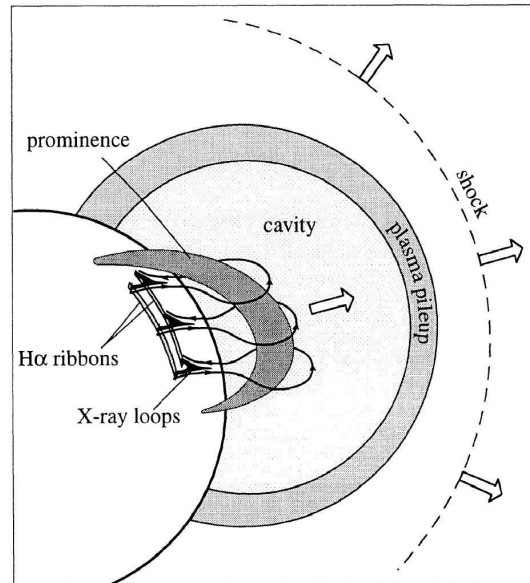
Figure 6. Representation by Forbes (2000) of what has become a standard model for a "three-part" CME or eruptive flare: a prominence and its surrounding cavity rise through the lower corona, followed by sequential magnetic reconnection and the formation of flare ribbons at the footpoint of a loop arcade.

First among these would be the problem of solar open flux (Gold, 1962; Crooker et al., 2002); CMEs regularly increase the fraction of solar open field, and have a strong solar-cycle occurrence pattern, so why doesn't the magnetic intensity in the heliosphere steadily increase? Second, the ejected magnetic flux is often twisted to form flux ropes, and these will transport magnetic helicity away from the Sun (Low, 1994; Kumar and Rust, 1996) – ultimately, from the interior dynamo itself.

References

Altschuler, M. D. and G. Newkirk: 1969, 'Magnetic Fields and the Structure of the Solar Corona. I: Methods of Calculating Coronal Fields'. *Solar Phys* **9**, 131.

Antiochos, S. K., C. R. Devore, and J. A. Klimchuk: 1999, 'A Model for Solar Coronal Mass Ejections'. *ApJ* **510**, 485–493.

Anzer, U. and G. W. Pneuman: 1982, 'Magnetic reconnection and coronal transients'. *Solar Phys* **79**, 129–147.

Athay, R. G. and G. E. Moreton: 1961, 'Impulsive Phenomena of the Solar Atmosphere. I. Some Optical Events Associated with Flares Showing Explosive Phase.'. *ApJ* **133**, 935.

Bastian, T. S., M. Pick, A. Kerdraon, D. Maia, and A. Vourlidas: 2001, 'The Coronal Mass Ejection of 1998 April 20: Direct Imaging at Radio Wavelengths'. *ApJL* **558**, L65–L69.

Bothmer, V. and R. Schwenn: 1994, 'Eruptive prominences as sources of magnetic clouds in the solar wind'. *Space Science Reviews* **70**, 215.

Buffington, A., B. V. Jackson, and P. P. Hick: 2003, 'Calculations for and laboratory measurements of a multistage labyrinthine baffle for SMEI'. In: *Innovative Telescopes and Instrumentation for Solar Astrophysics. Edited by Stephen L. Keil, Sergey V. Avakyan . Proceedings of the SPIE, Volume 4853, pp. 490-503 (2003).* pp. 490–503.

Burkepile, J. T., A. J. Hundhausen, A. L. Stanger, O. C. St. Cyr, and J. A. Seiden: 2004, 'Role of projection effects on solar coronal mass ejection properties: 1. A study of CMEs associated with limb activity'. *Journal of Geophysical Research (Space Physics)* pp. 3103.

Burlaga, L. F., L. Klein, N. R. Sheeley, D. J. Michels, R. A. Howard, M. J. Koomen, R. Schwenn, and H. Rosenbauer: 1982, 'A magnetic cloud and a coronal mass ejection'. *GRL* **9**, 1317–1320.

Cameron, R. and I. Sammis: 1999, 'Tangential Field Changes in the Great Flare of 1990 May 24'. *ApJL* **525**, L61–L64.

Chapman, S. and J. Bartels: 1940, *Geomagnetism*. Oxford: University Press.

Chen, P. F., S. T. Wu, K. Shibata, and C. Fang: 2002, 'Evidence of EIT and Moreton Waves in Numerical Simulations'. *ApJL* **572**, L99–L102.

Ciaravella, A., J. C. Raymond, J. Li, P. Reiser, L. D. Gardner, Y.-K. Ko, and S. Fineschi: 2002, 'Elemental Abundances and Post-Coronal Mass Ejection Current Sheet in a Very Hot Active Region'. *ApJ* **575**, 1116–1130.

Cremades, H. and V. Bothmer: 2004, 'On the three-dimensional configuration of coronal mass ejections'. *A&A* **422**, 307–322.

Crooker, N., J. Joselyn, and J. Feynman: 1997, *Coronal Mass Ejections: Causes and Consequences*. Geophysical Monographs #99.

Crooker, N. U., J. T. Gosling, and S. W. Kahler: 2002, 'Reducing heliospheric magnetic flux from coronal mass ejections without disconnection'. *Journal of Geophysical Research (Space Physics)* **107**, 3–1.

Dere, K. P. *et al.*: 1997, 'EIT and LASCO Observations of the Initiation of a Coronal Mass Ejection'. *Solar Phys* **175**, 601–612.

Forbes, T. G.: 2000, 'A review on the genesis of coronal mass ejections'. *JGR* **105**(14), 23153–23166.

Gary, G. A.: 2001, 'Plasma Beta above a Solar Active Region: Rethinking the Paradigm'. *Solar Phys* **203**, 71–86.

Gold, T.: 1962, 'Magnetic Storms'. *Space Science Reviews* **1**, 100.

Gopalswamy, N., M. Shimojo, W. Lu, S. Yashiro, K. Shibasaki, and R. A. Howard: 2003, 'Prominence Eruptions and Coronal Mass Ejection: A Statistical Study Using Microwave Observations'. *ApJ* **586**, 562–578.

Gosling, J. T.: 1991, 'In situ observations of coronal mass ejections in interplanetary space'. *NASA STI/Recon Technical Report N* **92**, 17725.

Gosling, J. T., S. J. Bame, D. J. McComas, J. L. Phillips, A. Balogh, and K. T. Strong: 1995, 'Coronal Mass Ejections at High Heliographic Latitudes: ULYSSES'. *Space Science Reviews* **72**, 133.

Gosling, J. T. and R. J. Forsyth: 2001, 'CME-Driven Solar Wind Disturbances at High Heliographic Latitudes'. *Space Science Reviews* **97**, 87–98.

Gosling, J. T., E. Hildner, R. M. MacQueen, R. H. Munro, A. I. Poland, and C. L. Ross: 1974, 'Mass ejections from the sun - A view from SKYLAB'. *JGR* **79**(18), 4581–4587.

Gosling, J. T., E. Hildner, R. M. MacQueen, R. H. Munro, A. I. Poland, and C. L. Ross: 1976, 'The speeds of coronal mass ejection events'. *Solar Phys* **48**, 389–397.

Gosling, J. T., D. J. McComas, J. L. Phillips, L. A. Weiss, V. J. Pizzo, B. E. Goldstein, and R. J. Forsyth: 1994, 'A new class of forward-reverse shock pairs in the solar wind'. *GRL* **21**, 2271–2274.

Hanaoka, Y., H. Kurokawa, S. Enome, H. Nakajima, K. Shibasaki, M. Nishio, T. Takano, C. Torii, H. Sekiguchi, S. Kawashima, T. Bushimata, N. Shinohara, Y. Irimajiri, H. Koshiishi, Y. Shiomi, Y. Nakai, Y. Funakoshi, R. Kitai, K. Ishiura, and G. Kimura: 1994, 'Simultaneous observations of a prominence eruption followed by a coronal arcade formation in radio, soft X-rays, and H(alpha)'. *PASJ* **46**, 205–216.

Handy, B. N., *et al.*,: 1999, 'The transition region and coronal explorer'. *Solar Phys.* **187**, 229–260.

Harra, L. K. and A. C. Sterling: 2001, 'Material Outflows from Coronal Intensity "Dimming Regions" during Coronal Mass Ejection Onset'. *ApJL* **561**, L215–L218.

Harrison, R. A., P. Bryans, G. M. Simnett, and M. Lyons: 2003, 'Coronal dimming and the coronal mass ejection onset'. *A&A* **400**, 1071–1083.

Harvey, K., N. Sheeley, and J. Harvey: 1986, 'HE I 10830 A Observations of Two-Ribbon Flare-Like Events Associated with Filament Disappearances'. In: *Solar-Terrestrial Predictions*. pp. 198.

Hildner, E., J. T. Gosling, R. T. Hansen, and J. D. Bohlin: 1975, 'The sources of material comprising a mass ejection coronal transient'. *Solar Phys* **45**, 363–376.

Hirayama, T.: 1974, 'Theoretical Model of Flares and Prominences. I: Evaporating Flare Model'. *Solar Phys* **34**, 323.

Howard, R. A., D. J. Michels, N. R. Sheeley, and M. J. Koomen: 1982, 'The observation of a coronal transient directed at earth'. *ApJL* **263**, L101–L104.

Howard, R. A., N. R. Sheeley, D. J. Michels, and M. J. Koomen: 1985, 'Coronal mass ejections - 1979-1981'. *JGR* **90**(9), 8173–8191.

Howard, R. A., N. R. Sheeley, D. J. Michels, and M. J. Koomen: 1986, 'The solar cycle dependence of coronal mass ejections'. In: *ASSL Vol. 123: The Sun and the Heliosphere in Three Dimensions*. pp. 107–111.

Hudson, H., B. Haisch, and K. T. Strong: 1995, 'Comment on 'The solar flare myth' by J. T. Gosling'. *JGR* **100**(9), 3473–3477.

Hudson, H. S.: 1991, 'Solar flares, microflares, nanoflares, and coronal heating'. *Solar Phys* **133**, 357–369.

Hudson, H. S., L. W. Acton, and S. L. Freeland: 1996, 'A Long-Duration Solar Flare with Mass Ejection and Global Consequences'. *ApJ* **470**, 629.

Hudson, H. S. and E. W. Cliver: 2001, 'Observing coronal mass ejections without coronagraphs'. *JGR* **106**, 25199–25214.

Hudson, H. S. and D. F. Webb: 1997, 'Soft X-ray signatures of coronal ejections'. *Geophysical Monographs #99* p. 27.

Hundhausen, A. J.: 1993, 'Sizes and locations of coronal mass ejections - SMM observations from 1980 and 1984-1989'. *JGR* **98**(17), 13177.

Hundhausen, A. J., J. T. Burkepile, and O. C. St. Cyr: 1994, 'Speeds of coronal mass ejections: SMM observations from 1980 and 1984-1989'. *JGR* **99**(18), 6543–6552.

Hundhausen, A. J., C. B. Sawyer, L. House, R. M. E. Illing, and W. J. Wagner: 1984, 'Coronal mass ejections observed during the solar maximum mission - Latitude distribution and rate of occurrence'. *JGR* **89**(18), 2639–2646.

Illing, R. M. E. and A. J. Hundhausen: 1985, 'Observation of a coronal transient from 1.2 to 6 solar radii'. *JGR* **90**(9), 275–282.

Innes, D. E., D. E. McKenzie, and T. Wang: 2003, 'SUMER spectral observations of post-flare supra-arcade inflows'. *Solar Phys* **217**, 247–265.

Jackson, B. V. and R. A. Howard: 1993, 'A CME Mass Distribution Derived from SOLWIND Coronagraph Observations'. *Solar Phys* **148**, 359.

Ji, H., H. Wang, E. J. Schmahl, Y.-J. Moon, and Y. Jiang: 2003, 'Observations of the Failed Eruption of a Filament'. *ApJL* **595**, L135–L138.

Kahler, S. W. and D. V. Reames: 1991, 'Probing the magnetic topologies of magnetic clouds by means of solar energetic particles'. *JGR* **96**(15), 9419–9424.

Kahler, S. W., D. V. Reames, and N. R. Sheeley: 2001, 'Coronal Mass Ejections Associated with Impulsive Solar Energetic Particle Events'. *ApJ* **562**, 558–565.

Kano, R.: 1994, 'The Time Evolution of X-Ray Structure during Filament Eruption'. In: *X-ray solar physics from Yohkoh*. pp. 273

Klimchuk, J. A., L. W. Acton, K. L. Harvey, H. S. Hudson, K. L. Kluge, D. G. Sime, K. T. Strong, and T. Watanabe: 1994, 'Coronal Eruptions Observed by *Yohkoh*'. In: *X-ray solar physics from Yohkoh*. pp. 181.

Ko, Y., J. C. Raymond, J. Lin, G. Lawrence, J. Li, and A. Fludra: 2003, 'Dynamical and Physical Properties of a Post-Coronal Mass Ejection Current Sheet'. *ApJ* **594**, 1068–1084.

Kumar, A. and D. M. Rust: 1996, 'Interplanetary magnetic clouds, helicity conservation, and current-core flux-ropes'. *JGR* **101**(10), 15667–15684.

Kundu, M. R.: 1965, *Solar radio astronomy*. New York: Interscience Publication, 1965.

Larson, D. E., R. P. Lin, J. M. McTiernan, J. P. McFadden, R. E. Ergun, M. McCarthy, H. Rème, T. R. Sanderson, M. Kaiser, R. P. Lepping, and J. Mazur: 1997, 'Tracing the topology of the October 18-20, 1995, magnetic cloud with $0.1 - 10^2$ keV electrons'. *GRL* **24**, 1911.

Low, B. C.: 1994, 'Magnetohydrodynamic processes in the solar corona: Flares, coronal mass ejections, and magnetic helicity'. *Physics of Plasmas* **1**, 1684–1690.

MacQueen, R. M. and R. R. Fisher: 1983, 'The kinematics of solar inner coronal transients'. *Solar Phys* **89**, 89–102.

McKenzie, D. E. and H. S. Hudson: 1999, 'X-Ray Observations of Motions and Structure above a Solar Flare Arcade'. *ApJL* **519**, L93–L96.

Melrose, D. B.: 1995, 'Current Paths in the Corona and Energy Release in Solar Flares'. *ApJ* **451**, 391.

Moore, R. L., A. C. Sterling, H. S. Hudson, and J. R. Lemen: 2001, 'Onset of the Magnetic Explosion in Solar Flares and Coronal Mass Ejections'. *ApJ* **552**, 833–848.

Moses, D., F. *et al.*,: 1997, 'EIT Observations of the Extreme Ultraviolet Sun'. *Solar Phys* **175**, 571–599.

Munro, R. H., J. T. Gosling, E. Hildner, R. M. MacQueen, A. I. Poland, and C. L. Ross: 1979, 'The association of coronal mass ejection transients with other forms of solar activity'. *Solar Phys* **61**, 201–215.

Nitta, N. and S. Akiyama: 1999, 'Relation between Flare-associated X-Ray Ejections and Coronal Mass Ejections'. *ApJL* **525**, L57–L60.

Pojoga, S. and T. S. Huang: 2003, 'On the sudden disappearances of solar filaments and their relationship with coronal mass ejections'. *Advances in Space Research* **32**, 2641–2646.

Raymond, J. C., A. Ciaravella, D. Dobrzycka, L. Strachan, Y.-K. Ko, M. Uzzo, and N. Raouafi: 2003, 'Far-Ultraviolet Spectra of Fast Coronal Mass Ejections Associated with X-Class Flares'. *ApJ* **597**, 1106–1117.

Rust, D. M.: 1979, 'Coronal manifestations of eruptive prominences - Observation and interpretation'. In: *IAU Colloq. 44: Physics of Solar Prominences*. pp. 252–266.

Rust, D. M. and A. Kumar: 1996, 'Evidence for Helically Kinked Magnetic Flux Ropes in Solar Eruptions'. *ApJL* **464**, L199.

Schatten, K. H., J. M. Wilcox, and N. F. Ness: 1969, 'A model of interplanetary and coronal magnetic fields'. *Solar Phys* **6**, 442–455.

Schmieder, B., L. van Driel-Gesztelyi, G. Aulanier, P. Démoulin, B. Thompson, C. de Forest, J. E. Wiik, C. Saint Cyr, and J. C. Vial: 2002, 'Relationships between CME's and prominences'. *Advances in Space Research* **29**, 1451–1460.

Schwenn, R.: 1986, 'Relationship of coronal transients to interplanetary shocks 3D aspects'. *Space Science Reviews* **44**, 139–168.

Schwenn, R.: 1995, 'Mass ejections from the sun and their interplanetary counterparts'. In: *Solar Wind Conference*. pp. 45.

Schwenn, R.: 1996, 'An Essay on Terminology, Myths and Known Facts: Solar Transient - Flare - CME - Driver Gas - Piston - BDE - Magnetic Cloud - Shock Wave - Geomagnetic Storm'. *APSS* **243**, 187

Sheeley, N. R., J. D. Bohlin, G. E. Brueckner, J. D. Purcell, V. E. Scherrer, R. Tousey, J. B. Smith, D. M. Speich, E. Tandberg-Hanssen, and R. M. Wilson: 1975, 'Coronal changes associated with a disappearing filament'. *Solar Phys* **45**, 377–392.

Sheeley, N. R., R. A. Howard, D. J. Michels, M. J. Koomen, R. Schwenn, K. H. Muehlhaeuser, and H. Rosenbauer: 1985, 'Coronal mass ejections and interplanetary shocks'. *JGR* **90**(9), 163–175.

Sheeley, N. R., J. H. Walters, Y.-M. Wang, and R. A. Howard: 1999, 'Continuous tracking of coronal outflows: Two kinds of coronal mass ejections'. *JGR* **104**, 452–462.

St. Cyr, O. C., J. T. Burkepile, A. J. Hundhausen, and A. R. Lecinski: 1999, 'A comparison of ground-based and spacecraft observations of coronal mass ejections from 1980-1989'. *JGR* **104**(13), 12493–12506.

St. Cyr, O. C., S. P. Plunkett, D. J. Michels, S. E. Paswaters, M. J. Koomen, G. M. Simnett, B. J. Thompson, J. B. Gurman, R. Schwenn, D. F. Webb, E. Hildner, and P. L. Lamy: 2000, 'Properties of coronal mass ejections: SOHO LASCO observations from January 1996 to June 1998'. *JGR* **105**(14), 18169–18186.

Sterling, A. C. and H. S. Hudson: 1997, '*Yohkoh* SXT Observations of X-Ray "Dimming" Associated with a Halo Coronal Mass Ejection'. *ApJL* **491**, L55.

Subramanian, P. and K. P. Dere: 2001, 'Source Regions of Coronal Mass Ejections'. *ApJ* **561**, 372–395.

Thompson, B. J., J. B. Gurman, W. M. Neupert, J. S. Newmark, J.-P. Delaboudinière, O. C. St. Cyr, S. Stezelberger, K. P. Dere, R. A. Howard, and D. J. Michels: 1999, 'SOHO/EIT Observations of the 1997 April 7 Coronal Transient: Possible Evidence of Coronal Moreton Waves'. *ApJL* **517**, L151–L154.

Tousey, R.: 1973, 'The Solar Corona'. In: M. J. Rycroft and S. K. Runcorn (eds.): *Space Research*. pp. 713.

Uchida, Y.: 1968, 'Propagation of Hydromagnetic Disturbances in the Solar Corona and Moreton's Wave Phenomenon'. *Solar Phys* **4**, 30.

Vourlidas, A., D. Buzasi, R. A. Howard, and E. Esfandiari: 2002, 'Mass and energy properties of LASCO CMEs'. In: *ESA SP-506: Solar Variability: From Core to Outer Frontiers*. pp. 91.

Vourlidas, A., P. Subramanian, K. P. Dere, and R. A. Howard: 2000, 'Large-Angle Spectrometric Coronagraph Measurements of the Energetics of Coronal Mass Ejections'. *ApJ* **534**, 456–467.

Wang, Y., S. H. Hawley, and N. R. Sheeley: 1996, 'The Magnetic Nature of Coronal Holes'. *Science* **271**, 464–469.

Webb, D. F. and R. A. Howard: 1994, 'The solar cycle variation of coronal mass ejections and the solar wind mass flux'. *JGR* **99**(18), 4201–4220.

Withbroe, G. L.: 1988, 'The temperature structure, mass, and energy flow in the corona and inner solar wind'. *ApJ* **325**, 442–467.

Zarro, D. M., A. C. Sterling, B. J. Thompson, H. S. Hudson, and N. Nitta: 1999, 'SOHO EIT Observations of Extreme-Ultraviolet "Dimming" Associated with a Halo Coronal Mass Ejection'. *ApJL* **520**, L139–L142.

Zhang, J., K. P. Dere, R. A. Howard, M. R. Kundu, and S. M. White: 2001, 'On the Temporal Relationship between Coronal Mass Ejections and Flares'. *ApJ* **559**, 452–462.